AIAA JOURNAL
Vol. 44, No. 10, October 2006

Analytical Electroacoustic Model of a Piezoelectric Composite Circular Plate

Suryanarayana A. N. Prasad,* Quentin Gallas,* Stephen Horowitz,* Brian Homeijer,*
Bhavani V. Sankar,† Louis N. Cattafesta,‡ and Mark Sheplak§
Interdisciplinary Microsystems Group, University of Florida, Gainesville, Florida 32611-6250

DOI: 10.2514/1.19855

This paper presents an analytical two-port, lumped-element model of a piezoelectric composite circular plate. In particular, the individual components of a piezoelectric unimorph transducer are modeled as lumped elements of an equivalent electrical circuit using conjugate power variables. The transverse static deflection field as a function of pressure and voltage loading is determined to synthesize the two-port dynamic model. Classical laminated plate theory is used to derive the equations of equilibrium for clamped circular laminated plates containing one or more piezoelectric layers. A closed-form solution is obtained for a unimorph device in which the diameter of the piezoelectric layer is less than that of the shim. Methods to estimate the model parameters are discussed, and model verification via finite-element analyses and experiments is presented. The results indicate that the resulting lumped-element model provides a reasonable prediction (within 3%) of the measured response to voltage loading and the natural frequency, thus enabling design optimization of unimorph piezoelectric transducers.

I. Introduction

MANY commonly used electroacoustic devices , such as microphones and headphones, employ circular disk transducers that are piezoelectric composite plates. Recent devices, such as synthetic jet actuators , used in flow control applications, can also be driven by piezoelectric composite circular plates. Micro-fluidic pump drivers represent another relatively new application for these devices [3]. The design of these transducers requires the development of analytical models to predict the electroacoustic behavior of the transducer elements. In addition, these transducers are often part of a larger, multi-energy domain, dynamic system. Therefore, a transfer function block is required to relate the input voltage to the output property of interest (e.g., volumetric flow rate).

A piezoelectric composite plate actuator or sensor represents a coupled electro-mechanical-acoustic system with frequency dependent properties determined by device dimensions and material properties. The analysis and design of coupled-domain transducer systems are commonly performed using lumped-element models [1,4]. The main assumption employed in lumped-element modeling (LEM) is that the characteristic length scales of the governing physical phenomena are much larger than the largest geometric dimension. For example, for the vibration of a piezoelectric composite plate, the bending wavelength and electromagnetic wavelength must be significantly larger than the device itself. If this quasistatic assumption holds, then the temporal and spatial variations can be decoupled. This decoupling permits the governing partial differential equations of the distributed system to be "lumped" into a set of coupled ordinary differential equations via the solution of the static equations. The resulting lumped parameter system is used to construct an equivalent electrical circuit. This approach provides a simple method to estimate the dynamic response of a piezoelectric composite plate for design and optimization purposes and is much simpler than a direct analytical or numerical finite-element model for estimation of the dynamic response. The quasistatic assumption limits the validity of LEM to frequencies just beyond the first fundamental natural frequency [1,4]. Despite this limitation, LEM is a useful tool because most electroacoustic transducers operate in the compliance-dominated frequency region or at resonance. For this study, the lumped-element parameters are determined from the transverse static response of the composite plate to uniform pressure loading and voltage applied across the piezoelectric composite.

Previous modeling work in the area of piezoelectric composite circular plates has mainly focused on structures that are symmetrically layered about the neutral axis, such as bimorph transducers or asymmetric composites in which all layers possess the same radius [5–9]. Adelman and Stavsky [5] formulated the problem of piezoelectric circular composite plates using Kirchoff's plate theory. The static behavior of metal-piezoceramic unimorphs and PZT-5H bimorphs containing silver electrodes was obtained. In their analysis, the radius of the piezoelectric layer was the same as that of the metallic layer. They found that the static displacement for a given applied electric field might be significantly different depending on the manner in which the plate is supported. Dobrucki and Pruchnicki [6] formulated the problem of a piezoelectric axisymmetric bimorph in the form of a shell of revolution, but used the finite-element method to obtain an approximate numerical solution. For the purpose of experimental verification of their results, they used a flat circular plate bimorph. Morris and Foster [3] performed optimization of a piezoelectric bimorph for a micropump driver application. They used the finite-element method to compute plate deflections. The effects of edge support conditions were discussed, and empirical equations were derived for the optimum actuator dimensions. Heyliger and Ramirez [7] investigated the free vibration characteristics of laminated composite piezoelectric plates using the weak form of the governing equations. Chang and Du [8] derived the dynamic equations of axisymmetric unimorph disk transducers (referred to as an asymmetric bimorph by the authors). Solutions for the deflection field were obtained by solving the resulting eigenvalue problem using the technique of Stavsky and Loewy [10]. Optimum configurations for maximum static displacement sensitivity were presented. Ha and Kim [9] used impedance and admittance matrices to numerically simulate the behavior of asymmetric piezoelectric annular bimorphs. Percin and Yakub [11] analyzed annular piezoelectric

Presented as Paper 1365 at the 43rd AIAA/ASME/ASCE/AHS/ASC Structures, Structural Dynamics, and Materials Conference, Denver, CO, 22–25 April 2002; received 2 September 2005; revision received 31 March 2006; accepted for publication 24 March 2006.

*Graduate Research Assistant, Department of Mechanical and Aerospace Engineering. Student Member AIAA.

†Professor, Department of Mechanical and Aerospace Engineering. Associate Fellow AIAA

‡Associate Professor, Department of Mechanical and Aerospace Engineering. Associate Fellow AIAA

§Associate Professor, Department of Mechanical and Aerospace Engineering; sheplak@ufl.edu. Associate Fellow AIAA.

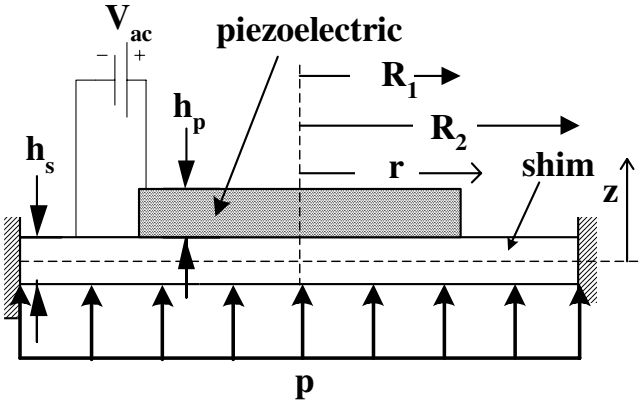

Fig. 1 A cross-sectional schematic of a clamped axisymmetric piezoelectric transducer.

disks for microelectromechanical systems-based ultrasound applications. They formulated the plate equations based on the classical (Kirchoff) plate theory for the first few modes and Mindlin plate theory for higher modes. They also suggested an equivalent circuit model for the transducer but limited their discussion to the electrical input impedance.

Many piezoelectric electroacoustic devices are not bimorphs possessing midplane symmetry. Such configurations may not be possible in all applications; i.e., access to electrical leads on both sides is often precluded. In such situations a unimorph transducer with a piezoceramic bonded to just one side of the structure is the only possible configuration. In addition, many commercially available piezoelectric unimorphs possess piezoelectric layers that do not cover the entire shim layer. Furthermore, many existing models result in numerical solutions rather than algebraic expressions and are computationally expensive for design optimization. Hence, there exists a need to develop a closed-form solution of the electroacoustic model for piezoelectric unimorphs.

This paper presents a two-port electroacoustic model of an axisymmetric piezoelectric unimorph transducer. The synthesis of the two-port model requires determination of the transverse static deflection field as a function of pressure and voltage loading. Classical laminated plate theory (CLPT) is used to derive the equations of equilibrium of circular laminated plates containing one or more piezoelectric layers. Figure 1 shows a cross-section of a typical clamped circular piezoelectric unimorph composite plate subjected to a uniform transverse pressure loading P and/or an applied voltage V_{ac}. The piezoceramic material possesses a thickness h_p and radius R_1. It is bonded to one side of a shim material possessing a radius R_2 and a thickness h_s. The pressure and/or voltage loading generates a transverse displacement field $w(r)$ and a radial displacement field $u(r, z)$ in the plate. In this paper, the equations are solved for a practical unimorph device wherein the diameter of the piezoelectric layer is less than that of the shim, i.e., $R_1 < R_2$ (see Fig. 1). Closed-form expressions for the deflection field as a function of the applied uniform pressure and/or the uniform electric field across the piezoelectric layer are found. The deflection field is then used to generate a two-port electroacoustic model of the unimorph transducer.

II. Two-Port Network Modeling

Ideally, a piezoelectric unimorph actuator/sensor is a linear, conservative, reciprocal transducer [4]. As an actuator, the piezoelectric composite diaphragm vibrates in response to an applied ac voltage. As a sensor, electrical charge is generated on the piezoelectric electrodes in response to pressure loading. Up to and just beyond the first resonant mode, the piezoelectric composite unimorph can be lumped into idealized discrete circuit elements using conjugate power variables. In this electroacoustic analogy, differential pressure and voltage are effort variables, whereas current and volumetric flow rate are flow variables. The resulting approximate piezoelectric coupling equations for this model are similar to those of a one-dimensional piezoelectric electromechanical coupling [1,4] and are written as

$$\begin{Bmatrix} \Delta\text{Vol} \\ q \end{Bmatrix} = \begin{bmatrix} C_{\text{AS}} & d_A \\ d_A & C_{\text{EF}} \end{bmatrix} \begin{Bmatrix} P \\ V_{\text{ac}} \end{Bmatrix} \tag{1}$$

where ΔVol is the volume displaced by the plate due to the application of differential pressure P and/or voltage V_{ac}, q is the charge stored on the piezoelectric electrodes, C_{EF} is the electrical free capacitance of the piezoelectric material, C_{AS} is the short-circuit acoustic compliance of the shim plate, and d_A is the effective acoustic piezoelectric coefficient of the assumed reciprocal transducer. The displaced volume is calculated by integrating the transverse displacement $w(r)$ over the entire plate area

$$\Delta\text{Vol} = \int_0^{R_2} 2\pi r w(r)\, \mathrm{d}r \tag{2}$$

The electrical free capacitance is the capacitance of the piezoelectric material in an unloaded or "free" state (i.e., $P = 0$)

$$C_{\text{EF}} = \frac{\varepsilon_r \varepsilon_0 \pi R_1^2}{h_p} \tag{3}$$

where ε_r is the relative dielectric constant of the piezoelectric material and ε_0 is the permittivity of free space. The short-circuit acoustic compliance is determined by integrating the transverse diaphragm displacement generated by a unit pressure loading with the piezoelectric layer electrically shorted:

$$C_{\text{AS}} = \left.\frac{\Delta\text{Vol}}{P}\right|_{V_{\text{ac}}=0} = \frac{\int_0^{R_2} w(r)|_{V_{\text{ac}}=0} 2\pi r\, \mathrm{d}r}{P} \tag{4}$$

Similarly, the effective acoustic piezoelectric coefficient is most easily determined from the volumetric displacement due solely to an applied voltage:

$$d_A = \left.\frac{\Delta\text{Vol}}{V_{\text{ac}}}\right|_{P=0} = \frac{\int_0^{R_2} w(r)|_{P=0} 2\pi r\, \mathrm{d}r}{V_{\text{ac}}} \tag{5}$$

The piezoelectric coupling equations are written in conjugate power-variable form by assuming sinusoidal steady state operating conditions, i.e., replacing P and V_{ac} in Eq. (1) by $Pe^{j\omega t}$ and $V_{\text{ac}}e^{j\omega t}$, respectively, and differentiating Eq. (1) with respect to time,

$$\begin{Bmatrix} Q \\ i \end{Bmatrix} = \begin{bmatrix} j\omega C_{\text{AS}} & j\omega d_A \\ j\omega d_A & j\omega C_{\text{EF}} \end{bmatrix} \begin{Bmatrix} P \\ V_{\text{ac}} \end{Bmatrix} \tag{6}$$

where

$$Q = \int_0^{R_2} 2\pi r \frac{\mathrm{d}w(r)}{\mathrm{d}t}\, \mathrm{d}r = \frac{\mathrm{d}(\Delta\text{Vol})}{\mathrm{d}t} = j\omega\Delta\text{Vol} \tag{7}$$

is the volume velocity, $i = \dot{q}$ is the current, and ω is the frequency in radians per second.

In LEM, the coupling between the two different energy domains is realized by using equivalent two-port models [4]. For this paper, we employ an impedance analogy, in which elements that share a common effort are connected in parallel, whereas those sharing a common flow are connected in series. Because an ideal piezoelectric unimorph is an indirect, conservative transducer, the two-port model can be represented by a transformer with a parallel shunt capacitance attached to the electrical port and a series compliance attached to the mechanical port as shown in Fig. 2.

The parameter ϕ, also called the transformer turns ratio in the equivalent circuit representation, is the electroacoustic transduction coefficient. This coefficient is defined as the negative ratio of the effective acoustic piezoelectric coefficient and the short-circuit acoustic compliance of the plate,

$$\phi = -\frac{d_A}{C_{\text{AS}}} \tag{8}$$

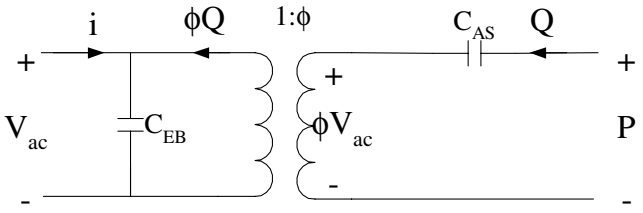

Fig. 2 Equivalent two-port circuit representation of piezoelectric transduction.

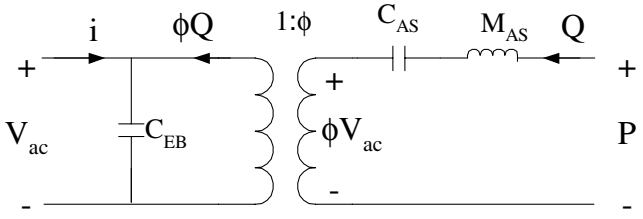

Fig. 3 Equivalent two-port circuit representation of axisymmetric piezoelectric unimorph disk.

The blocked electrical capacitance is related to the free capacitance by

$$C_{\mathrm{EB}} = C_{\mathrm{EF}}(1 - k^2) \tag{9}$$

where k^2 is the electroacoustic energy-coupling factor,

$$k^2 = \frac{d_A^2}{C_{\mathrm{EF}} C_{\mathrm{AS}}} \tag{10}$$

This coefficient provides an indication of the electroacoustic energy conversion efficiency for the unimorph transducer but does not yield the actual efficiency because it does not account for electrical and mechanical losses as well as electrical and mechanical loads [1].

The equivalent circuit in Fig. 2 is exact in the static limit as $\omega \to 0$, but an effective short-circuit acoustic mass, M_{AS}, must be added in series with the acoustic compliance as shown in Fig. 3 to accurately approximate the dynamic behavior up to just beyond the first resonant frequency [4]. The acoustic mass is determined by equating the lumped kinetic energy of the electrically shorted vibrating diaphragm expressed in acoustic conjugate power variables to the total kinetic energy,

$$M_{\mathrm{AS}} = 2\pi \int_0^{R_2} \rho_A \left(\frac{w(r)}{\Delta \mathrm{Vol}} \bigg|_{V_{\mathrm{ac}}=0} \right)^2 r \, \mathrm{d}r \tag{11}$$

where ρ_A is the areal density of the piezoelectric composite plate ($\mathrm{kg/m^2}$),

$$\rho_A = \int_{z_1}^{z_2} \rho \, \mathrm{d}z \tag{12}$$

and ρ is the density of the corresponding layer.

The short-circuit resonant frequency f_S of the lumped-element model of the piezoelectric unimorph is

$$f_S = \frac{1}{2\pi \sqrt{C_{\mathrm{AS}} M_{\mathrm{AS}}}} \tag{13}$$

The lumped-element model is an idealized representation that does not take into account mechanical dissipation due to structural damping or acoustic radiation. It also does not take into account the dielectric losses in the piezoelectric material. Depending on the application of the unimorph, these losses can be represented by parallel and/or series resistors attached to the mechanical and electrical ports [1].

III. Electromechanical Plate Model

The synthesis of the two-port, lumped-element model outlined in the preceding section requires the determination of the short-circuit acoustic compliance, Eq. (4), the effective acoustic piezoelectric coefficient, Eq. (5), and the short-circuit acoustic mass, Eq. (11). All of these quantities depend on the electromechanical behavior of the piezoelectric composite plate.

The equilibrium equations [12–14] of the axisymmetric plate shown in Fig. 1 are

$$\frac{\mathrm{d}N_r}{\mathrm{d}r} + \frac{N_r - N_\theta}{r} = 0 \tag{14}$$

$$Q_r = \frac{\mathrm{d}M_r}{\mathrm{d}r} + \frac{M_r - M_\theta}{r} \tag{15}$$

and

$$\frac{\mathrm{d}Q_r}{\mathrm{d}r} + P + \frac{Q_r}{r} = 0 \tag{16}$$

where N_r and N_θ are the force resultants in the radial and circumferential directions, respectively. Similarly, M_r and M_θ are the moment resultants, and Q_r is the transverse shear force resultant. The number of equilibrium equations can be reduced to two by substituting for Q_r from Eq. (15) into Eq. (16) to obtain

$$\frac{1}{r}\frac{\mathrm{d}}{\mathrm{d}r}\left(r\frac{\mathrm{d}M_r}{\mathrm{d}r} + M_r - M_\theta \right) + P = 0 \tag{17}$$

The radial and circumferential strain-displacement relationships from Kirchoff's plate theory are

$$\varepsilon_{rr} = \varepsilon_{rr}^0 + z\kappa_r \tag{18}$$

and

$$\varepsilon_{\theta\theta} = \varepsilon_{\theta\theta}^0 + z\kappa_\theta \tag{19}$$

where $\kappa_r = -(\mathrm{d}^2 w/\mathrm{d}r^2) = -(\mathrm{d}\theta/\mathrm{d}r)$ and $\kappa_\theta = -(1/r)(\mathrm{d}w/\mathrm{d}r) = -(\theta/r)$ are the radial and circumferential curvatures, respectively, and θ is the transverse deflection slope. The strains in the reference plane ($z = 0$) are

$$\varepsilon_{rr}^0 = \frac{\mathrm{d}u_0}{\mathrm{d}r} \tag{20}$$

and

$$\varepsilon_{\theta\theta}^0 = \frac{u_0}{r} \tag{21}$$

The constitutive equations for a transversely isotropic, linear elastic axisymmetric piezoelectric plate are

$$\begin{Bmatrix} \sigma_{rr} \\ \sigma_{\theta\theta} \end{Bmatrix} = [Q]\left(\begin{Bmatrix} \varepsilon_{rr}^0 \\ \varepsilon_{\theta\theta}^0 \end{Bmatrix} + z\begin{Bmatrix} \kappa_r \\ \kappa_\theta \end{Bmatrix} - E_f \begin{Bmatrix} d_{31} \\ d_{31} \end{Bmatrix} \right) \tag{22}$$

where

$$[Q] = \frac{E}{1 - \nu^2}\begin{Bmatrix} 1 & \nu \\ \nu & 1 \end{Bmatrix} \tag{23}$$

E is the Young's modulus, and ν is Poisson's ratio. The last term in Eq. (22) is due to the piezoelectric effect, where $E_f = V_{\mathrm{ac}}/h_p$ is the electric field strength for an electrically conductive shim, and d_{31} is the piezoelectric modulus. The explicit z-dependence of the material properties is understood and is omitted here for convenience.

The force and moment resultants are obtained by integrating the constitutive equations through the thickness of the composite plate, resulting in

$$\begin{Bmatrix} N_r \\ N_\theta \end{Bmatrix} = [A]\begin{Bmatrix} \varepsilon_{rr}^0 \\ \varepsilon_{\theta\theta}^0 \end{Bmatrix} + [B]\begin{Bmatrix} \kappa_r \\ \kappa_r \end{Bmatrix} - \begin{Bmatrix} N_r^P \\ N_\theta^P \end{Bmatrix} \tag{24}$$

and

$$\begin{Bmatrix} M_r \\ M_\theta \end{Bmatrix} = [B]\begin{Bmatrix} \varepsilon^0_{rr} \\ \varepsilon^0_{\theta\theta} \end{Bmatrix} + [D]\begin{Bmatrix} \kappa_r \\ \kappa_\theta \end{Bmatrix} - \begin{Bmatrix} M^P_r \\ M^P_\theta \end{Bmatrix} \tag{25}$$

where

$$[A] = \int_{z_1}^{z_2} [Q]\,\mathrm{d}z \tag{26}$$

is the extensional stiffness matrix,

$$[B] = \int_{z_1}^{z_2} [Q]z\,\mathrm{d}z \tag{27}$$

is the flexural-extensional coupling matrix, and

$$[D] = \int_{z_1}^{z_2} [Q]z^2\,\mathrm{d}z \tag{28}$$

is the flexural stiffness matrix. In the preceding expressions, z_1 is the z location of the bottom of the composite, and z_2 represents the z location of the top of the composite. As shown in Fig. 1, the reference plane was chosen to be at the middle of the shim material to simplify the annular plate solution.

The piezoelectric coupling generates both force and moment resultants that are given by

$$\begin{bmatrix} N^P_r \\ N^P_\theta \end{bmatrix} = \int_{z_1}^{z_2} E_f[Q]\begin{bmatrix} d_{31} \\ d_{31} \end{bmatrix}\mathrm{d}z \tag{29}$$

and

$$\begin{bmatrix} M^P_r \\ M^P_\theta \end{bmatrix} = \int_{z_1}^{z_2} E_f[Q]\begin{bmatrix} d_{31} \\ d_{31} \end{bmatrix} z\,\mathrm{d}z \tag{30}$$

The governing equations for a piezoelectric composite plate are derived by substituting for the force and moment resultants from Eqs. (29) and (30) into the equilibrium equations, Eqs. (14) and (17). Then the strain and curvature terms are replaced by displacement $u_0(r)$ and slope $\theta(r)$ to obtain the two equilibrium equations in terms of $u_0(r)$ and $\theta(r)$ as

$$\frac{\mathrm{d}^2\theta(r)}{\mathrm{d}r^2} + \frac{1}{r}\frac{\mathrm{d}\theta(r)}{\mathrm{d}r} - \frac{\theta(r)}{r^2} = -\frac{Pr}{2D^*_{11}} \tag{31}$$

and

$$\frac{\mathrm{d}^2u_0(r)}{\mathrm{d}r^2} + \frac{1}{r}\frac{\mathrm{d}u_0(r)}{\mathrm{d}r} - \frac{u_0(r)}{r^2} = -\frac{Pr\alpha}{2D^*_{11}} \tag{32}$$

where $\alpha = B_{11}/A_{11}$ and the reduced bending stiffness is $D^*_{11} = [D_{11} - (B^2_{11}/A_{11})]$.

The specific problem shown in Fig. 1 is solved by combining the homogenous annular plate solution with the solution of the inner piezoelectric composite plate of radius R_1. Equations (31) and (32) are thus valid for both the inner circular and outer annular regions. In the inner piezoelectric composite plate region, the electric field is not a function of r; therefore the piezoelectric force and moment resultants are constant. As a result, the piezoelectric coupling does not explicitly appear in the governing displacement equations, but arises from the matching conditions at the interface ($r = R_1$). The general solutions to Eqs. (31) and (32) are

$$\theta(r) = b_1 r + \frac{b_2}{r} - \frac{1}{D^*_{11}}\left(\frac{Pr^3}{16}\right) \tag{33}$$

and

$$u_0 = a_1 r + \frac{a_2}{r} - \frac{\alpha}{D^*_{11}}\left(\frac{Pr^3}{16}\right) \tag{34}$$

where a_1, a_2, b_1, and b_2 are arbitrary constants. The inner and outer solutions require the determination of eight constants via boundary conditions and interface matching conditions. The boundary conditions consist of finite values at the origin and clamped conditions at the support:

$$\theta(0) < \infty \tag{35}$$

$$u_0(0) < \infty \tag{36}$$

$$u_0(R_2) = 0 \tag{37}$$

and

$$\theta(R_2) = 0 \tag{38}$$

The interface compatibility conditions between the inner circular composite plate and the outer annular plate are

$$\theta^{(1)}(R_1) = \theta^{(2)}(R_1) \tag{39}$$

$$u^{(1)}_0(R_1) = u^{(2)}_0(R_1) \tag{40}$$

$$N^{(1)}_r(R_1) = N^{(2)}_r(R_1) \tag{41}$$

and

$$M^{(1)}_r(R_1) = M^{(2)}_r(R_1) \tag{42}$$

where the superscripts (1) and (2) denote the central composite plate and annular shim regions, respectively. The piezoelectric coupling is introduced by the piezoelectric contributions to the integrated force, Eq. (29), and moment, Eq. (30), resultants in the matching conditions at the interface Eqs. (41) and (42).

The transverse deflection $w_0(r)$ is calculated by first integrating the slope $\theta(r)$ with respect to the radius in each of the regions and then by applying the clamped boundary condition and the matching conditions at the interface. The resulting expressions for transverse deflection for the inner and outer regions are

$$w^{(1)}_0(r) = b^{(1)}_1\left(\frac{r^2 - R^2_1}{2}\right) - \frac{P(r^4 - R^4_1)}{64D^{*(1)}_{11}} + b^{(2)}_1\left[\frac{R^2_1 - R^2_2}{2} - R^2_2\,\ell_n\left(\frac{R_1}{R_2}\right)\right] + \frac{P}{64D^{(2)}_{11}}\left[4R^4_2\,\ell_n\left(\frac{R_1}{R_2}\right) - R^4_1 + R^4_2\right] \tag{43}$$

and

$$w^{(2)}_0(r) = b^{(2)}_1\left[\frac{r^2 - R^2_2}{2} - R^2_2\,\ell_n\left(\frac{r}{R_2}\right)\right] + \frac{P}{64D^{(2)}_{11}}\left[4R^4_2\,\ell_n\left(\frac{r}{R_2}\right) - r^4 + R^4_2\right] \tag{44}$$

respectively. The expressions for the constants are found in the Appendix and the complete details of the solution are given in Prasad . The short-circuit acoustic compliance is then obtained from Eq. (4):

$$C_{AS} = \frac{2\pi}{P}\left[b^{(1)}_1\left(\frac{-R^4_1}{8}\right) + b^{(2)}_1\left(\frac{(R^2_2 - R^2_1)^2}{8}\right) + \frac{PR^6_1}{192D^{*(1)}_{11}} + \frac{PR^2_1(-R^4_1 + 3R^4_2 - 2R^6_2/R^2_1)}{192D^{(2)}_{11}}\right]\Bigg|_{V=0} \tag{45}$$

The effective acoustic piezoelectric coefficient is obtained from Eq. (5):

$$d_A = \frac{2\pi}{V}\left[b^{(1)}_1\left(\frac{-R^4_1}{8}\right) + b^{(2)}_1\left(\frac{(R^2_2 - R^2_1)^2}{8}\right)\right]\Bigg|_{P=0} \tag{46}$$

The expression for the acoustic mass [Eq. (11)] does not possess a closed-form solution and is obtained via numerical integration.

Table 1 Properties of APC 850 device

Geometric properties	
Outer radius R_2	11.5 mm
Radius of piezoelectric R_1	10.0 mm
Radius of silver	9.2 mm
Thickness of shim h_s	0.20 mm
Thickness of piezoelectric h_p	0.23 mm
Thickness of silver	1 μm
Material properties	
Elastic modulus of shim E_s	90 GPa
Poisson's ratio of shim ν_s	0.32
Density of shim ρ_s	8700 kg/m^3
Elastic modulus of piezoelectric E_p	63 GPa
Poisson's ratio of piezoelectric ν_p	0.31
Density of piezoelectric ρ_p	7700 kg/m^3
Electrical properties	
Relative dielectric constant ε_r	1750
Piezoelectric constant d_{31}	−175 pm/V

IV. Model Validation and Parameter Extraction

Both numerical simulations and experiments are used in to validate the two-port lumped-element model. The devices used are commercially available circular piezoelectric unimorphs (APC International Ltd.—Model APC 850) whose characteristics are summarized in Table 1.

First, a finite-element (FE) analysis of the structure is performed to validate whether CLPT is appropriate to model a device. As noted previously, the composite plate can respond to two types of loading: voltage and/or pressure. A FE analysis is then independently performed in Abaqus for both loading situations. The shim plate is modeled using eight-node biquadratic axisymmetric solid elements having the transverse and radial displacements as degrees of freedom (DOF), whereas the piezoceramic is modeled using eight-node biquadratic axisymmetric piezoelectric quadrilaterals having the transverse and radial displacements and electrical potential as DOF. The electric potential DOF is only active during the voltage loading analysis. A grid resolution study yielded a total of 110×3 elements used for the piezoelectric part and 130×4 elements to accurately model the shim. The elements are clustered near the edge of the piezoelectric patch where maximum shear stress occurs. Because axisymmetric elements are employed, a symmetric boundary condition (BC) is applied at the middle plane section and the edge of the shim surface has a perfectly clamped BC. Furthermore, a perfect bond is assumed between the piezoceramic and the shim. Because the FE model uses solid elements, the converged solution may be considered as exact. Figures 4 and 5 show excellent agreement between the plate theory deflection and the FE results for both pressure and voltage loading analysis, respectively. This indicates that the geometry, material properties, and support conditions of the device allow use of CLPT in the present case.

Next, an experimental investigation is performed to further validate the ability of the analytical model to predict dynamic effects. The transverse deflection of the clamped piezoelectric composite plate is acquired via a Polytec PI scanning laser vibrometer (MSV200), as shown in Fig. 6, and the measured velocity is integrated in the frequency domain to obtain displacement. The frequency response of the diaphragm center is first acquired, in which the device is excited by a low voltage (5 V amplitude) periodic chirp signal with frequencies ranging from 200 to 4000 Hz. The results, shown in Fig. 7, are representative of a typical second-order underdamped system with a damping ratio $\zeta \cong 0.007$ and reveals that the fundamental natural frequency $f_d = 3505$ Hz compares favorably with the predicted short-circuit natural frequency via Eq. (13) of $f_s = 3542$ Hz. The measured f_d frequency is slightly different from the predicted f_s due to the finite source impedance of the function generator. Note that an empirical acoustic resistance $R_{\mathrm{AS}} = 2\zeta\sqrt{M_{AS}/C_{AS}}$ can be inserted in series with C_{AS} and M_{AS} in Fig. 3 to account for acoustic radiation and inherent structural damping.

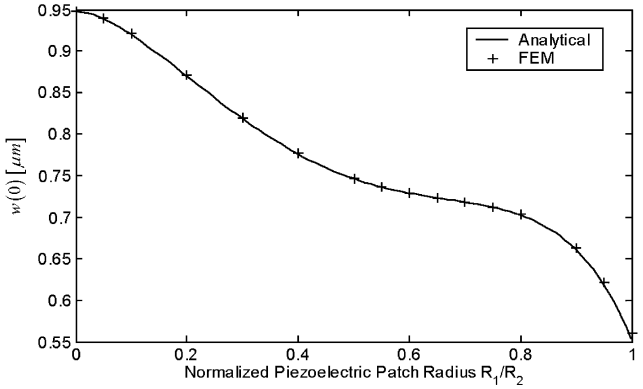

Fig. 4 Comparison of center deflection for different radii of the piezoelectric material as predicted by the analytical solution and finite-element model for unit pressure loading with $V_{\mathrm{ac}} = 0$ and $h_p/h_s = 0.4$.

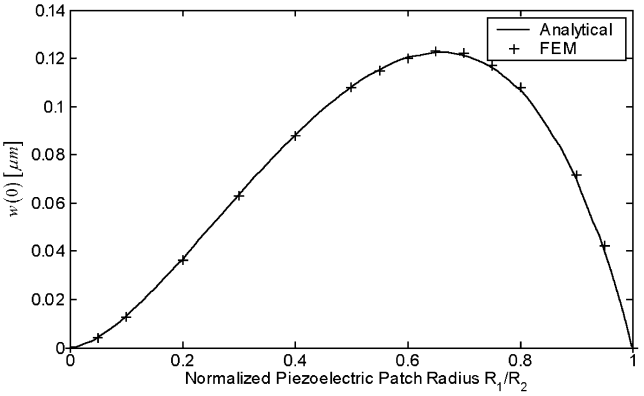

Fig. 5 Comparison of center deflection for different radii of the piezoelectric material as predicted by the analytical solution and finite-element model for a unit voltage loading with $P = 0$ and $h_p/h_s = 0.4$.

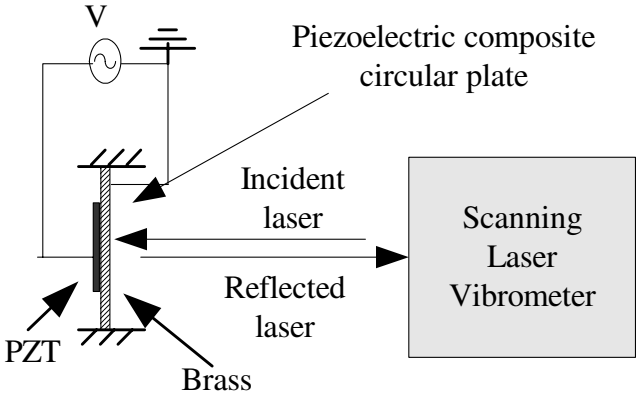

Fig. 6 Schematic of the experimental setup showing the scanning laser vibrometer focused on the clamped PZT unimorph transducer being excited by a sinusoidal voltage.

Next, to determine the mode shape of the piezoelectric diaphragm at low frequencies, the scanning laser vibrometer is again used, where the radius of the diaphragm is scanned every 0.6 mm and a fixed input sinusoidal voltage of 5 V at 100 Hz is applied across the piezoceramic. As shown in Fig. 7, this frequency is sufficiently close to dc to represent the static response of the composite diaphragm and to allow a direct comparison with the predicted analytical model response. The comparison is shown in Fig. 8, where fair agreement is obtained between the linear static mode shape predicted by the analytical model and the experimental data. Uncertainty estimates of the frequency response function are calculated and shown in the figure in accordance with the procedures outlined in Bendat and Piersol [16].

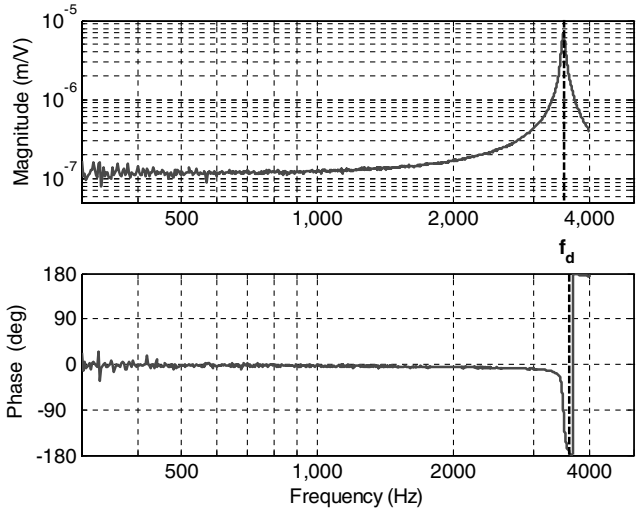

Fig. 7 Measured displacement frequency response function at $r = 0$ obtained by integrating velocity measurements.

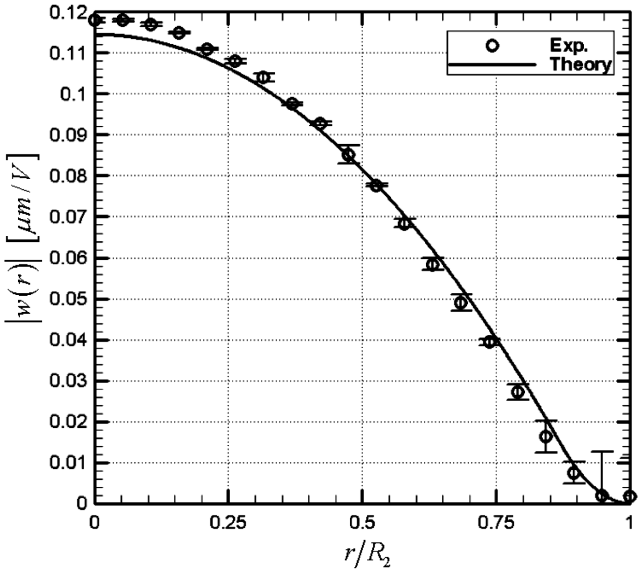

Fig. 8 Comparison between the measured mode shape at 100 Hz and the static linear composite plate theory.

The present theory is used to extract the lumped-element parameters used in the two-port network model. Table 2 summarizes the results. The lumped-element model predicts the experimental resonant frequency shown in Fig. 5 to within 3%. The error in the prediction of the center transverse deflection is also approximately 3%. This implies that the effective acoustic piezoelectric coefficient, which is a function of the transverse deflection and mode shape, also matches well.

The results from the experiments and numerical simulations confirm the validity of the linear electroacoustic model presented in this paper. However, some limitations of this model need to be pointed out. First, the effects of the bond layer between the piezoelectric and the shim layers, as well as the silver electrode, are neglected in the current analytical model. Additional FE analyses and experiments have shown that the silver layer (having a thickness on the order of 1 μm) does not significantly affect the performance of the device in terms of mode shape and stress distribution. On the other hand, the effect of the bond layer (having a thickness on the order of 25 μm) is negligible only when the thickness of the piezoceramic is at least a few times greater than the bond layer. In addition, the axisymmetric assumption implies that the circular piezoceramic patch is bonded in the center of the shim, and the commercially available unimorphs exhibit some nonuniformity in this regard. Finally, it should be emphasized that an ideal clamped boundary is difficult to achieve in practice. In our setup, thick clamp plates are used in conjunction with several uniformly spaced bolts around the circumference, and uniform clamping pressure is assured via a torque wrench. Nonetheless, despite these limitations, the two-port electroacoustic model presented in this paper is shown to yield a valid prediction of the dynamic response of the piezoelectric composite plate actuator for design and optimization purposes.

Table 2 Lumped-element model parameters

Parameter	Theory	Experiment	Error, %
ϕ	138.3 Pa/V	——	——
C_{AS}	1.5243×10^{-13} m^{4}s^2/kg	——	——
M_{AS}	13456 kg/m^4	——	——
d_A	-2.1080×10^{-11} m^3/V	——	——
C_{EF}	21.155 nF	——	——
C_{EB}	18.239 nF	——	——
k^2	0.1378	——	——
f_s	3514.1 Hz	——	——
f_d	——	3505 Hz	0.3
$\frac{w_0(0)\|_{P=0}}{V_{\mathrm{ac}}}$	0.1163 μm/V	0.1182 μm/V	1.6

V. Results and Discussion

Using the validated model, the general effects of pressure and electrical loading are now studied in greater detail. For the pressure-loading case, the nondimensional center deflection, $\bar{w}_P(0)$, is obtained via normalization of $w_P(0)$ by the corresponding value for a homogeneous plate with the same radius, thickness, and material properties of the shim

$$\bar{w}_P(0) = \frac{w_P(0)}{PR_2^4/64D_{11}^{(2)}} = \frac{w_P(0)/R_2}{\frac{3}{16}(1-\nu_s^2)(P/E_s)(R_2/h_s)^3} \tag{47}$$

where $D_{11}^{(2)} = D_s = E_s h_s^3/12(1-\nu_s^2)$ is the flexural rigidity of the shim, and the subscript P denotes pressure loading. The main advantage associated with this choice is that the nondimensional deflection is dependent only on the ratio of the radii, thickness and Young's modulus of the piezoceramic material and the shim

$$\bar{w}_P(0) = f\left(\frac{E_p}{E_s}, \frac{h_p}{h_s}, \frac{R_1}{R_2}\right) \tag{48}$$

The parameter ν_p/ν_s does not vary sufficiently to be a design parameter.

The best way to illustrate the device behavior is to plot the nondimensional center deflection against the radius ratio R_1/R_2 for different values of h_p/h_s and for a fixed E_p/E_s as shown in Fig. 9. The value of Young's modulus ratio $E_p/E_s = 0.7$ (Brass/PZT) corresponds to the APC 850 piezoceramic unimorph transducer. The results demonstrate that the theory correctly reverts to homogeneous plate behavior as the nondimensional piezoceramic radius R_1/R_2 and thickness h_p/h_s approach zero. Furthermore, as R_1/R_2 and h_p/h_s increase due to increase piezoceramic patch size, the nondimensional center deflection due to pressure loading decreases as expected due to the increased stiffness of the device.

Similarly for an applied voltage, the center deflection is nondimensionalised by the product of the piezoelectric modulus, the piezoelectric radius and the critical electric field $E_{f_{\mathrm{crit}}}$

$$\bar{w}_V(0) = \frac{w_V(0)}{E_{f_{\mathrm{crit}}} d_{31} R_2} \tag{49}$$

where $E_{f_{\mathrm{crit}}} = 30$ V/mil is a typical coercive field for PZT and the subscript V denotes an applied voltage. Nondimensionalizing by electric field, and not by applied voltage, was selected in Eq. (49) for optimization purposes. In practice, it is likely that a large (or near coercive) electric field will be imposed as an operational constraint. Furthermore, the typical design problem is to maximize $\bar{w}_V(0)$ by

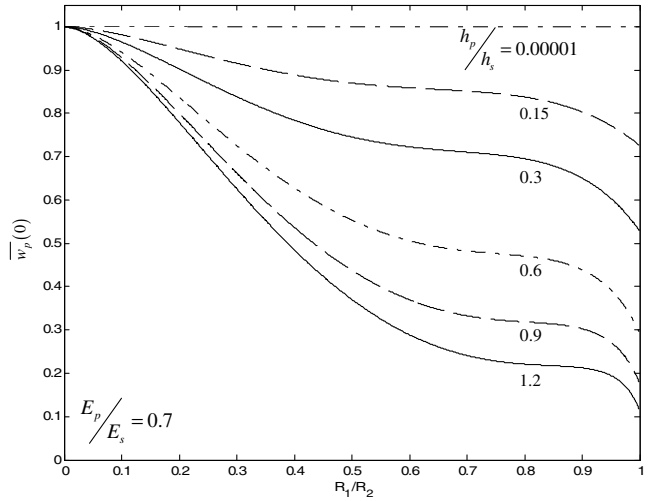

Fig. 9 Nondimensional deflection plot for $E_p/E_s = 0.7$ when only pressure is applied for various thickness ratios.

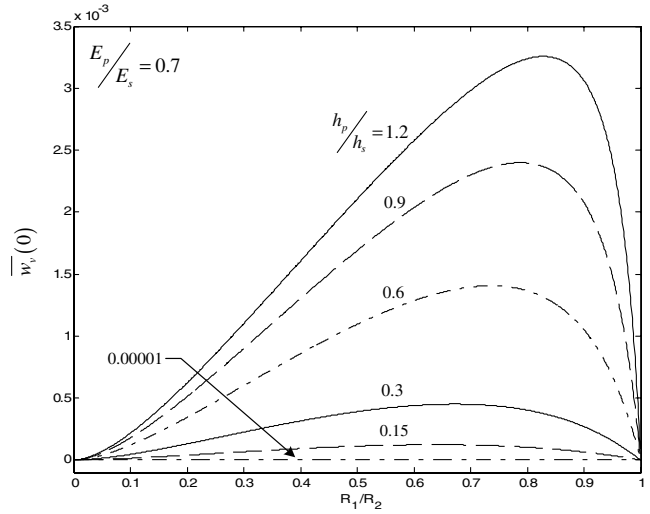

Fig. 10 Nondimensional deflection plot for $E_p/E_s = 0.7$ when only voltage is applied for various thickness ratios.

varying the piezoceramic dimensions for a prescribed shim radius R_2. The nondimensional deflection is again dependent only on the ratios of the radius, thickness, and Young's modulus

$$\bar{w}_V(0) = f\left(\frac{E_p}{E_s}, \frac{h_p}{h_s}, \frac{R_1}{R_2}\right) \tag{50}$$

As before, the best way to illustrate this behavior is to plot the nondimensional center deflection versus the radius ratio R_1/R_2 for different values of h_p/h_s and for $E_p/E_s = 0.7$. Figure 10 reveals several interesting features. First, for a given thickness ratio h_p/h_s, there exists an optimum piezoceramic patch radius to maximize the deflection due to an applied voltage. As h_p/h_s increases from 0 to 1.2, $\bar{w}_V(0)$ monotonically increases and the optimum value of R_1/R_2 increases from approximately 0.65 to 0.85. In contrast to a piezoelectric cantilever unimorph, the assumption of a clamped boundary condition forces $\bar{w}_V(0) \equiv 0$ when the piezoelectric material covers the entire shim. In practice, the boundary condition will possess finite compliance, and hence will result in a finite deflection.

VI. Conclusions

This paper presents an analytic two-port, lumped-element model of an axisymmetric piezoelectric unimorph transducer. LEM provides a compact analytical model and valuable physical insight into the dependence of the device behavior on geometry and material properties. The synthesis of the two-port model requires determination of the transverse static deflection field as a function of linear pressure and voltage loading. Classical laminated plate theory is used to derive the equations of equilibrium for clamped circular laminated plates containing one or more piezoelectric layers. The equations are solved for a unimorph device wherein the diameter of the piezoelectric layer is less than that of the shim. The model is validated using both finite-element analyses with separate pressure and voltage loading and experiments with voltage loading. In particular, the natural frequency inferred from the lumped-element model compares favorably with the experiments. Limitations of the model are discussed.

The nondimensional center deflection depends only on the radius and thickness ratios of the piezoceramic to the shim as well as the material properties. In terms of application, the derived analytical expressions of the lumped-element parameters will be useful for modeling, design, and optimization of transducer systems that use unimorphs. Specifically, this model has already been employed in the electroacoustic model of synthetic jet actuators [2].

Appendix: Solution Constants

The constants involved in the general solution are obtained by substituting the boundary and interface matching conditions in the general solution [15]. They are listed here:

$$a_1^{(2)} = \frac{\beta}{(1 - R_2^2/R_1^2)}\left((B_{11}^{(1)} + B_{12}^{(1)})\gamma + \left\{D_{11}^{(2)}\left[\left(\frac{R_1^2 + R_2^2}{R_1^2 - R_2^2}\right) + \nu_s\right] - (D_{11}^{(1)} + D_{12}^{(1)})\right\}\zeta\right) \tag{A1}$$

$$b_1^{(2)} = \frac{-\beta}{(1 - R_2^2/R_1^2)}\left((B_{11}^{(1)} + B_{12}^{(1)})\zeta + \left\{A_{11}^{(2)}\left[\left(\frac{R_1^2 + R_2^2}{R_1^2 - R_2^2}\right) + \nu_s\right] - (A_{11}^{(1)} + A_{12}^{(1)})\right\}\gamma\right) \tag{A2}$$

$$a_2^{(2)} = -a_1^{(2)} R_2^2 \tag{A3}$$

$$b_2^{(2)} = -b_1^{(2)} R_2^2 - \frac{P R_2^4}{16 D_{11}^{(2)}} \tag{A4}$$

$$a_1^{(1)} = a_1^{(2)}\left(1 - \frac{R_2^2}{R_1^2}\right) + \frac{P^* \alpha^{(1)}}{D_{11}^{*(1)}} \tag{A5}$$

$$b_1^{(1)} = b_1^{(2)}\left(1 - \frac{R_2^2}{R_1^2}\right) - \frac{P^*}{D_{11}^{(2)}}\left(1 - \frac{R_2^4}{R_1^4} - \frac{D_{11}^{(2)}}{D_{11}^{*(1)}}\right) \tag{A6}$$

$$a_2^{(1)} = 0 \tag{A7}$$

and

$$b_2^{(1)} = 0 \tag{A8}$$

where

$$\beta = P^*\left(\left\{D_{11}^{(2)}\left[\left(\frac{R_1^2 + R_2^2}{R_1^2 - R_2^2}\right) + \nu_s\right] - (D_{11}^{(1)} + D_{12}^{(1)})\right\} \times \left\{A_{11}^{(2)}\left[\left(\frac{R_1^2 + R_2^2}{R_1^2 - R_2^2}\right) + \nu_s\right] - (A_{11}^{(1)} + A_{12}^{(1)})\right\} - (B_{11}^{(1)} + B_{12}^{(1)})^2\right)^{-1} \tag{A9}$$

$$\gamma = \frac{B_{11}^{(1)}\alpha^{(1)} - D_{11}^{(1)}}{D_{11}^{*(1)}} + \frac{D_{11}^{(1)} + D_{12}^{(1)}}{D_{11}^{(2)}}\left(1 - \frac{R_2^4}{R_1^4}\right) - \nu_s - \frac{R_2^4}{R_1^4}(1 - \nu_s) - \frac{M^P}{P^*} \tag{A10}$$

$$\zeta = \frac{B_{11}^{(1)} + B_{12}^{(1)}}{D_{11}^{(2)}}\left(1 - \frac{R_2^4}{R_1^4}\right) + \frac{\alpha^{(1)}A_{11}^{(1)} - B_{11}^{(1)}}{D_{11}^{*(1)}} - \frac{N^P}{P^*} \tag{A11}$$

and

$$P^* = \frac{PR_1^2}{16} \tag{A12}$$

Acknowledgments

The authors gratefully acknowledge support from NASA Langley Research Center (grant nos. NAG-1-2261 and NAG-1-2249 monitored by M. G. Jones and S. Gorton, respectively).

References

[1] Rossi, M., *Acoustics and Electroacoustics*, Artechhouse, Norwood, MA, 1988, pp. 245–373.

[2] Gallas, Q., Holman, R., Nishida, T., Carroll, B., Sheplak, M., and Cattafesta, L., "Lumped Element Modeling of Piezoelectric-Driven Synthetic Jet Actuators," *AIAA Journal*, Vol. 41, No. 2, 2003, pp. 240–247.

[3] Morris, C. J., and Forster, F. K., "Optimization of a Circular Piezoelectric Bimorph for a Micropump Driver," *Journal of Micromechanics and Microengineering*. Vol. 10, Feb 2000, pp. 459–465.

[4] Merhaut, J., *Theory of Electroacoustics*, McGraw–Hill, New York, 1981, Chap. 6.

[5] Adelman, N. T., and Stavsky, Y., "Flexural-Extensional Behavior of Composite Piezoelectric Circular Plates," *Journal of the Acoustical Society of America*, Vol. 67, No. 3, 1980, pp. 819–822.

[6] Dobrucki, B., and Pruchnicki, P., "Theory of Piezoelectric Axisymmetric Bimorph," *Sensors and Actuators A (Physical)*, Vol. 58, No. 3, 1997, pp. 203–212.

[7] Heyliger, P. R., and Ramirez, G., "Free Vibration of Laminated Circular Piezoelectric Plates and Discs," *Journal of Sound and Vibration*, Vol. 229, No. 4, 2000, pp 935–956.

[8] Chang, S. H., and Du, B. C., "Optimization of Axisymmetric Bimorphic Disk Transducers," *Journal of the Acoustical Society of America*, Vol. 109, No. 1, 2001, pp. 194–202.

[9] Ha, S. K., and Kim, Y. H., "Analysis of an Asymmetrical Piezoelectric Annular Bimorph Using Impedance and Admittance Matrices," *Journal of the Acoustical Society of America*, Vol. 110, No. 1, 2001, pp. 208–215.

[10] Stavsky, Y., and Loewy, R., "Axisymmetric Vibrations of Isotropic Composite Circular Plates," *Journal of the Acoustical Society of America*, Vol. 49, No. 5(2), 1971, pp. 1542–1550.

[11] Percin, G., and Khuri-Yakub, B. T., "Piezoelectrically Actuated Flextensional Micromachined Ultrasound Transducers-I: Theory," *IEEE Transactions on Ultrasonics, Ferroelectrics, and Frequency Control*, Vol. 49, No. 5, 2002, pp. 573–584.

[12] Timoshenko, S. P., and Krieger, S. W., *Theory of Plates and Shells*, McGraw–Hill, New York, 1959.

[13] Reddy, J. N., *Theory and Analysis of Elastic Plates*, Taylor and Francis, London, 1999.

[14] Timoshenko, S. P., and Goodier, J. N., *Theory of Elasticity*, McGraw–Hill, New York, 1990.

[15] Prasad, S. A. N., "Two-Port Electroacoustic Model of Piezoelectric Composite Circular Plate," M.S. Thesis, Dept. of Aerospace Engineering, Mechanics, and Engineering Science, Univ. of Florida, Gainesville, FL, 2002.

[16] Bendat, J. S., and Piersol, A. G., *Random Data: Analysis and Measurement Procedures*, 3rd ed., Wiley-Interscience, New York, 2000, Chap. 8.

A. Roy
Associate Editor